

RAPID COMMUNICATION

Atomistic simulations of graphene origami: Dynamics and kinetics

To cite this article: Panpan Zhang *et al* 2023 *Chinese Phys. B* **32** 087107

View the [article online](#) for updates and enhancements.

You may also like

- [Origami-based earthworm-like locomotion robots](#)
Hongbin Fang, Yetong Zhang and K W Wang
- [The potential of DNA origami to build multifunctional materials](#)
Kosti Tapio and Ilko Bald
- [Development and modeling of multi-phase polymeric origami inspired architecture by using pre-molded geometrical features](#)
Mohamed Ali E Kshad and Hani E Naguib

Atomistic simulations of graphene origami: Dynamics and kinetics

Panpan Zhang(张盼盼)^{1,2,†}, Haihong Jia(贾海洪)^{1,2,†}, Yan-Fang Zhang(张艳芳)^{1,‡}, and Shixuan Du(杜世萱)^{1,2,3,§}

¹Institute of Physics and University of Chinese Academy of Sciences, Chinese Academy of Sciences, Beijing 100190, China

²Beijing National Laboratory for Condensed Matter Physics, Beijing 100190, China

³Songshan Lake Materials Laboratory, Dongguan 523808, China

(Received 5 April 2023; revised manuscript received 11 May 2023; accepted manuscript online 12 May 2023)

Origami offers two-dimensional (2D) materials with great potential for applications in flexible electronics, sensors, and smart devices. However, the dynamic process, which is crucial to construct origami, is too fast to be characterized by using state-of-the-art experimental techniques. Here, to understand the dynamics and kinetics at the atomic level, we explore the edge effects, structural and energy evolution during the origami process of an elliptical graphene nano-island (GNI) on a highly ordered pyrolytic graphite (HOPG) substrate by employing steered molecular dynamics simulations. The results reveal that a sharper armchair edge is much easier to be lifted up and realize origami than a blunt zigzag edge. The potential energy of the GNI increases at the lifting-up stage, reaches the maximum at the beginning of the bending stage, decreases with the formation of van der Waals overlap, and finally reaches an energy minimum at a half-folded configuration. The unfolding barriers of elliptical GNIs with different lengths of major axis show that the major axis should be larger than 242 Å to achieve a stable single-folded structure at room temperature. These findings pave the way for pursuing other 2D material origami and preparing origami-based nanodevices.

Keywords: origami process, dynamics and kinetics, structure and energy evolution, stability of single-folded structure

PACS: 71.15.Pd, 71.15.Mb, 71.15.Nc

DOI: 10.1088/1674-1056/acd527

1. Introduction

Origami effectively shapes two-dimensional (2D) materials into complex three-dimensional (3D) structures.^[1–4] The origami-inspired structures exhibit novel properties, such as the strong magneto-photoelectric effect,^[5] tunable chirality,^[6] Chern insulator with light irradiation,^[7] the coexistence of valley polarization and inversion,^[8] and unusual thermal properties.^[9–11] Therefore, origami structures have potential applications in wearable electronics,^[12] biological sensors,^[3] photodetection, imaging,^[13] etc. Among the variety of 2D materials, graphene has particular advantages in origami owing to its atomically thin thickness and extremely low bending stiffness.^[14] Previous studies reported that graphene could be folded by a contact-free atomic force microscope (AFM) tip^[15] or scanning tunneling microscope (STM) tip.^[16,17] In addition, graphene origami occurs with external stimuli such as temperature,^[18–20] light,^[21] strain,^[2,22] doping,^[23] solvent,^[24] and also spontaneously due to the formation of joint edges in the growth process.^[25] Chen *et al.* realized the atomically precise and direction-controllable folding of graphene nano island (GNI) using an STM tip at ultra-low temperature.^[17] To optimize origami protocols, it is essential to elucidate the dynamics and kinetics at atomic level and understand the key factors that control the folding. This is, how-

ever, very challenging, as the process is too fast to be characterized by using state-of-the-art experimental techniques.

Many efforts have been devoted to investigating the possibility of graphene origami using molecular dynamics. It includes the origami induced by hydrogenation,^[26,27] surface-functionalization,^[28] crease,^[29] scanning probe microscope tips,^[15–17] etc. Researchers reported the feasibility and critical size of a half fold and a French fold by combining static atomistic computations with a continuum model.^[30] However, the dynamics and kinetics at the atomic level, including the evolution of structure and energy during the folding process, the critical force to realize origami, and the stability of the folded graphene nano islands, which are crucial to controllable folding and further application, are still lacking.

In this work, the dynamics and kinetics of GNIs origami are explored by using steered molecular dynamic simulations (SMD) at an atomic level. SMD has been extensively used to investigate DNA folding/unfolding,^[31] force-activated molecular isomerization,^[32] etc. We use ellipse-shaped GNIs with minor/major axis ratios (L_b/L_a) of 1/2 in all the simulations. We find that the GNIs with armchair edges require smaller critical forces to be lifted up than those with zigzag edges. Moreover, a sharper edge requires a smaller critical force than the blunt ones. The GNI reaches the lowest energy state as the half-folded GNI is constructed. By analyzing the structure

[†]These authors contributed equally to this work.

[‡]Corresponding author. E-mail: zhangyanfang@ucas.ac.cn

[§]Corresponding author. E-mail: sxdu@iphy.ac.cn

and energy evolution during the origami process, we find that the unfolding is determined by the competition between the van der Waals (vdW) interaction in stacked regions and the deformation energy in the curved region. Since the deformation energy does not change much during folding, the system will be stabilized as the size of the stacked region increases. Radial distribution functions (RDFs) of the curved region and the variation of bond lengths show that the integrity of the GNI is well preserved during the whole origami process, suggesting the robust conjugated feature of GNI. We further evaluate the stability of folded GNIs of different sizes whose lengths of the long axis (L_a) range from 60 Å to 400 Å at room temperature (RT). It turns out that the major-axis length of GNI should be larger than 242 Å in order to realize a stable single-folded structure without the help of an external force.

2. Methods

The SMD simulations using the constant-force method are performed to study the origami process of GNI on a highly ordered pyrolytic graphite (HOPG) substrate. The ellipse-shaped GNI with $L_a = 301$ Å on a four-layer HOPG substrate is constructed to investigate the edge effects. To obtain the critical force of GNI origami, a series of SMD simulations under different constant forces are carried out. All SMD simulations are conducted under NVT ensembles at 1 K. To test the stability of the folded GNIs at room temperature, classic MD simulations of the folded GNIs with various major axis lengths

(60 Å–400 Å) are performed at 1 K and 300 K, respectively.

We use the general Amber force field (GAFF)^[33] to describe the inter- and intramolecular interaction parameters of GNI and the HOPG substrate. The simulations are carried out with three-dimensional periodic boundary conditions using the leapfrog integrator with a time step of 1.0 fs. Van der Waals interactions are calculated at a cutoff distance of 12 Å. The bottom layer of the HOPG substrate is fixed in all simulations. The v-rescale thermostat is chosen to control the temperature. All MD simulations are carried out using GROMACS-5.1.2 package.^[34]

3. Results and discussion

3.1. Structural evolution in origami process

The structural evolution of GNI origami is shown in Fig. 1, including single-folding and z -folding. Firstly, we put an ellipse-shaped GNI stacking on a HOPG substrate since graphene origami with GNI in elliptical and round shapes has been experimentally realized on HOPG.^[17] The major axis of the GNI is about 300 Å, while the minor axis is about 150 Å. L_a (L_b) represents the length of the major (minor) axis. The ratio of L_b/L_a equals 1/2 for all GNIs in this work. Then the GNI origami process is explored by constant-force SMD simulations under NVT ensemble at 1 K. A constant force (F) has been applied at the end of the GNI with a direction indicated as red arrows in Fig. 1.

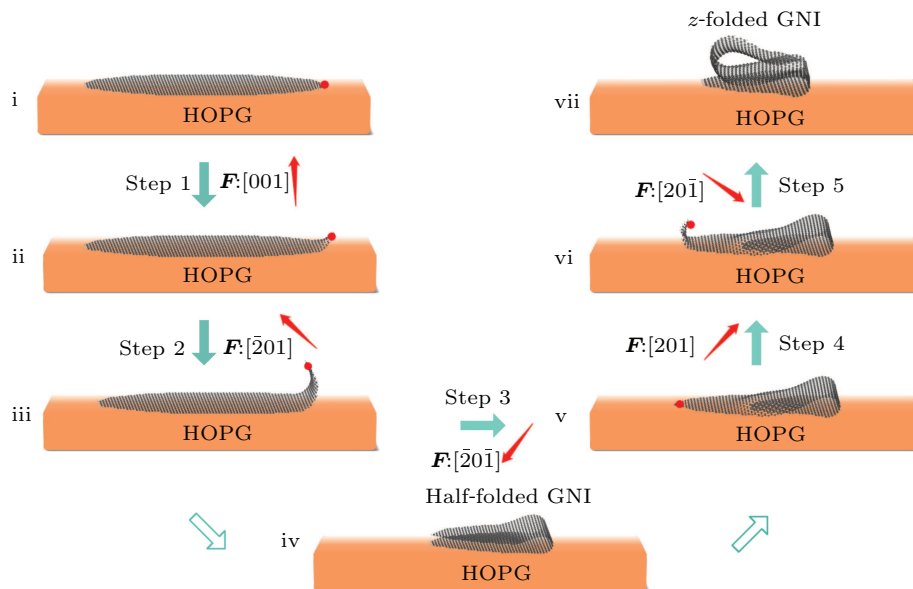


Fig. 1. The structural evolution of GNI origami. Single-folding and z -folding processes are realized after these simulation steps. Moss green arrows connect the initial and final structures in every simulation step. The two hollow arrows represent the formation of the half-folded GNI in step 3. The red arrows show the direction of the force (F) applied in each simulation step.

In step 1, a force along [001] is applied at one end (the red dot in Fig. 1i) of the ellipse-shaped GNI for 1 ns. A vertical force here is necessary to detach GNI away from HOPG, rather than forces in other directions (such as $[\bar{2}01]$ in step

2), making GNI slide on HOPG. The GNI eventually achieves equilibrium (Fig. 1ii) in step 1. Then, the direction of the force is changed, making the lifted side move further away from the substrate (step 2). When the center of mass of the pulled re-

gion is higher than a particular height (Fig. 1iii), the GNI is bent downward and continues to move leftward with force in $[\bar{2}0\bar{1}]$ direction, realizing a folded structure shown in Fig. 1v (step 3). A half-folded GNI (Fig. 1iv) is obtained during this step. Here, the minimal force to realize folding is denoted as a critical force (F_c , Fig. S1a in the ESM). The lifted height of the center of mass of the pulled region is denoted as h . At the beginning of step 3 (Fig. 1iii), the minimal h to realize folding under an external force is shortened to h_c (Fig. S1b in the ESM). z -folded GNI is achieved by repeating steps 2 and 3 as indicated in Figs. 1vi and 1vii. The line profile of the z -folded structure (Fig. S2 in the ESM) shows that the heights of single-folded and z -folded areas are 6.7 Å and 10.1 Å, respectively, which agree well with those reported in experiments (7.0 Å and 10.5 Å, respectively).^[17,35] The agreement between the simulated and the experimental results prove that the force field we used is good enough to reproduce the experimental process. Therefore, we use this force field to do further simulations and understand the dynamic process at an atomic scale based on the simulation results.

3.2. Edge effects on GNI origami

Firstly, we investigate the edge effect on the origami process with the pulling force applied on the GNI edge. Here, zigzag and armchair edges are considered since the previous work showed that the folded graphene along these two edges is more prevailing.^[36] The geometric structures of the two GNIs with armchair and zigzag edges, i.e., AGNI and ZGNI, on HOPG are shown in Figs. 2(a) and 2(b), respectively. For comparison, both GNIs have 13826 carbon atoms. The L_{as} of the two GNIs are 301 Å and 303 Å. Both GNIs are asymmetric with a sharp edge and a blunt edge, as shown in the zoom-in configurations of Fig. 2. There are three and nine carbon rings at the sharp edge and blunt edge, respectively. For simplicity, we use AGNI3 (AGNI9) to denote an AGNI with a sharp (blunt) edge, while ZGNI3 (ZGNI9) for ZGNI. The constant pulling force is applied on carbon atoms at one of the ends marked as red dots in the zoom-in structures in Fig. 2.

A successful folding requires an external force larger than F_c and the h higher than h_c . Here, h_c decreases with the increase of F while F is larger than F_c (see Fig. S1b). The F_c for AGNI3, AGNI9, ZGNI3, and ZGNI9 are 0.747 eV/Å, 0.811 eV/Å, 0.772 eV/Å, and 0.996 eV/Å, respectively (Fig. S1a). Comparing AGNI and ZGNI with the same width, the F_c for an armchair edge, for example, AGNI3, is lower than that of a zigzag edge, ZGNI3. For the same GNI, the F_c of AGNI3 (ZGNI3) is smaller than that of AGNI9 (ZGNI9). We then conclude that the GNI with an armchair edge is easier to realize folding, and a sharper edge is friendly for the folding for both armchair and zigzag edges.

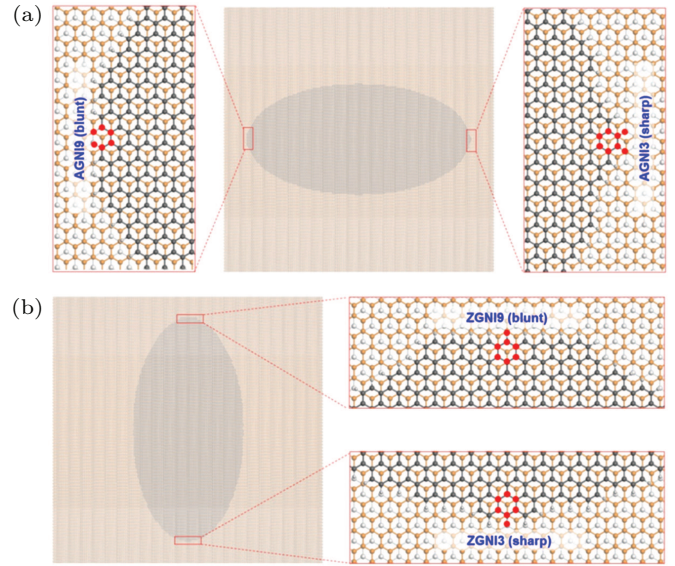


Fig. 2. Structures of GNIs with armchair and zigzag edges on a four-layer HOPG substrate. The GNIs with armchair (a) and zigzag (b) edge structures along the major axis. Pulling forces are applied at the region marked by red dots in the zoom-in figures. The carbon atoms in GNI, the top layer, and the bottom three layers of the HOPG substrate are colored in grey, orange, and light grey, respectively. Hydrogen atoms in GNIs are in light grey, while the balls are smaller than those representing carbon atoms.

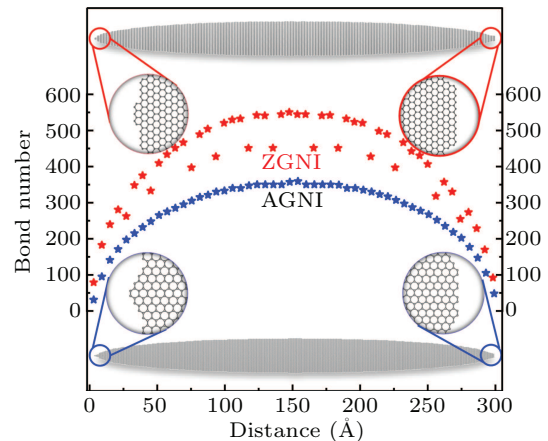


Fig. 3. Number of C–C bonds non-vertical to the folding direction along the major axis of GNIs. Red and blue stars denote the numbers of bonds non-vertical to the major axis of ZGNI and AGNI, respectively. The top and bottom panels are corresponding configurations of ZGNI and AGNI, respectively. For simplicity, only carbon atoms are considered and shown here.

Carbon–carbon (C–C) bonds non-vertical to the major axis will impede the folding process since the folding direction is along the major axis. To reveal the influence of the configuration of different edges on the GNI origami, we plot the distribution of the C–C bonds along the major axis of AGNI and ZGNI (Fig. 3). Only the C–C bonds that are non-vertical to the major axis have been counted. The distance in Fig. 3 begins at sharp edges (left) and ends at blunt edges (right) for both AGNI and ZGNI. Both major axes of AGNI and ZGNI are divided into 50 segments. For either AGNI or ZGNI, the sharp edge has fewer C–C bonds than the blunt edge. Taking the ZGNI as an example, the sharp edge (left) consists of 79

C–C bonds, while 92 bonds for the blunt edge (right) within a length of 6 Å. Thus, to lift and fold a GNI, a sharper edge needs a smaller critical force, in accordance with the previous results. In addition, the number of C–C bonds non-vertical to the major axis in the AGNI is smaller than that in the ZGNI along the major axis, indicating that the critical force for AGNI origami is smaller than that for ZGNI.

3.3. The potential energy evolution in GNI origami process

The GNI origami process follows steps 3–5 in Fig. 1. Since the evolution of potential energy (E_p) and the corresponding configuration are beneficial to understanding the complex dynamics of the origami process, we analyze the evolution of E_p s for the whole system and for the GNI (Fig. S3 in the ESM). Here the GNI with L_a of 301 Å is used as an example. The potential evolution in the z -folding process (steps 4 and 5 in Fig. 1) is similar to that in the single-folding process (steps 2 and 3 in Fig. 1). Therefore, we focus on the single-folding process shown in Fig. 4(a). In step 1, the ver-

tex where the force is applied is pulled ~ 1 Å away from its original position to equilibrium. The E_p of the GNI and that of the whole system remain almost unchanged (red and black curves, respectively).

In step 2, the GNI is pulled away from the substrate under a force along $[\bar{2}01]$ direction. Detaching the GNI from the HOPG substrate reduces the vdW stacking region and decreases the effective interaction between the GNI and the substrate, leading to an increase of E_p of the whole system. Meanwhile, as the curved region increases, strain occurs in more and more C–C bonds. Therefore, the E_p s of the GNI and the whole system increase. In step 3, the vertex is bent down and approaches the GNI region still on the substrate, resulting in a bilayer GNI region and a half-tube region. Thus, at the beginning of step 3, the evolution of E_p should be derived from the competition among three factors, the increasing vdW interaction inside GNI, the decreasing vdW interaction between the GNI and the HOPG substrate, and the increasing deformation energy of the half-tube region.

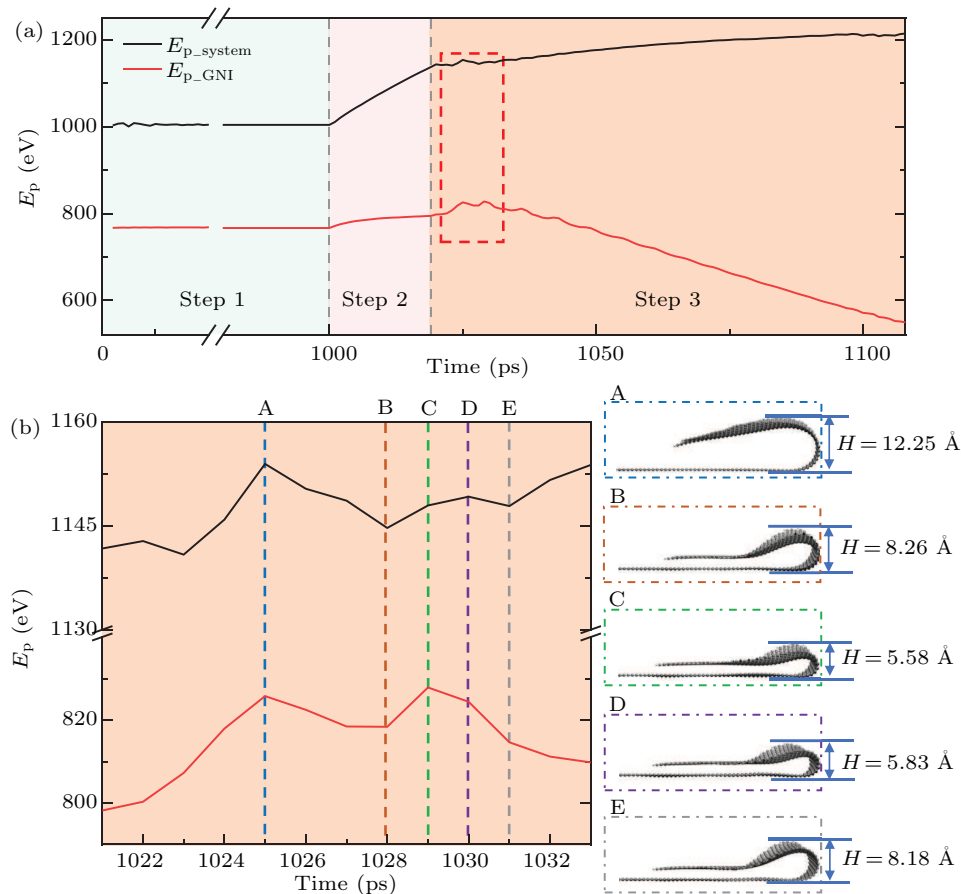


Fig. 4. The E_p evolution and corresponding configurations in the single-folding process. (a) The potential energy of the system (black curve) and that of the GNI (red curve) as a function of simulation time. Different colors in the background indicate different simulation steps. (b) A magnified view of the E_p s in the red dashed rectangle in (a). The vertical dashed lines indicate a particular simulation time. The corresponding configurations of GNI are shown in the right panel.

The first factor decreases the E_p of the GNI, while the other two factors increase the E_p of the GNI. The competition results in potential-energy peaks in the folding process indicated by the red dashed rectangle in Fig. 4(a) and highlighted

in Fig. 4(b). The E_p s of GNI and the whole system exhibit peaks at 1025 ps (dashed line A). The GNI forms a curved region (right panel of Fig. 4(b)) with a height of ~ 12.25 Å. The height of the curved region is much larger than the well-known

interlayer distance of graphite ($\sim 3.4 \text{ \AA}$) and the equilibrium height of the half-tube ($H_e \sim 7.2 \text{ \AA}$, see Fig. S4 in the ESM). The stain in the curved region leads to a high E_p state. As the folding continues, the bilayer region forms with the interlayer distance decreasing to about 3.4 \AA at 1028 ps (dashed line B). Meanwhile, the half-tube height (H) decreases to 8.26 \AA . The effective vdW interaction results in a low E_p state.

Next, the GNI enters another high E_p state at 1029 ps (dashed line C), which is caused by the small $H \sim 5.58 \text{ \AA}$ in configuration C (right panel of Fig. 4(b)). At 1030 ps (dashed line D), the H is almost unchanged, while the AB stacking area of the bilayer region increases (see Fig. S5 in the ESM). The increased AB stacking area inside the folded GNI lowers the E_p of GNI (see Fig. S6 in the ESM). Therefore, the E_p of GNI decreases slightly while the E_p of the system continues to increase. At 1031 ps (dashed line E), the curved region evolves close to its equilibrium ($\sim 8.18 \text{ \AA}$) with a decreased deformation energy. Thus, the E_p s of both GNI and the system decrease. In the following process, the H vibrates around the H_e , while the E_p of the GNI decreases as the bilayer region expands. We notice that the E_p of the whole system keeps increasing though that of the GNI decreases in step 3, indicating that an external force is necessary during the folding process.

3.4. Structural changes in the GNI origami process

The sp^2 hybridization of the carbon atoms is crucial for the folded GNIs to retain their properties. The 1.40 \AA bond length corresponds to the representative C–C bond in graphene. We then calculate the normalized radial distribution functions (RDFs)^[37] of the curved region of the half- and z-folded AGNI and compare them with the RDF of an unfolded AGNI. Figures 5(a) and 5(b) show the top and side views of half- and z-folded AGNI. The corresponding RDFs are plotted in Fig. 5(c). The RDF of the unfolded GNI shows the first peak at 1.40 \AA and the second one at 2.42 \AA , which are attributed to the distances between the nearest neighboring C atoms and the next nearest neighbors, respectively. The bond lengths in the curved regions are close to those in the unfolded GNI. Thus, the sp^2 hybridization of the carbon atoms in curved regions is reserved after GNI origami.

In addition, the RDF peaks of the curved regions are relatively broader than those of the unfolded GNI, demonstrating that some of the C–C bonds are slightly stretched or compressed. We then investigate the variation of bond length during the origami process. The maximum, minimum, and average values of C–C and carbon-hydrogen (C–H) bond lengths as a function of simulation time are shown in Fig. S7. The C–C bond lengths range from 1.36 \AA to 1.44 \AA , very close to those in the unfolded GNI (1.40 \AA), suggesting that all the carbon atoms are still sp^2 hybridized. The lengths of the C–H bonds vary slightly between 1.07 \AA and 1.10 \AA . By comparing the

RDFs and bond-length evolution in the folded and unfolded GNI, we find that the origami process neither induces the formation of new chemical bonds nor breaks the preexisting C–C bonds. The sp^2 hybridization nature of the GNI remains after origami.

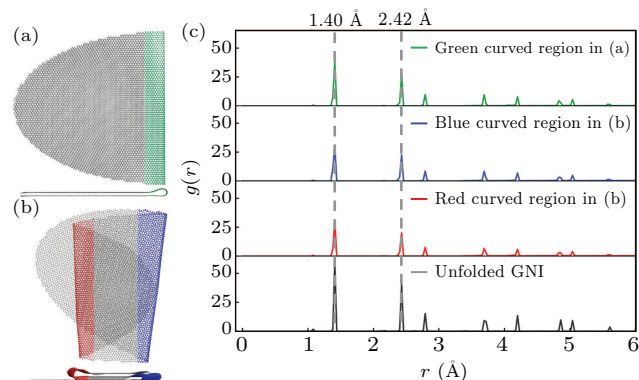


Fig. 5. RDFs of the folded and unfolded GNI. (a) and (b) Top and side views of half- and z-folded GNI. The curved area of half-folded GNI is colored green. Blue and red represent the lower and upper curved regions in a z-folded GNI. (c) RDFs of the curved and unfolded regions in GNI. The gray line is the RDF of an unfolded GNI. Green, blue, and red lines denote the corresponding RDFs of the curved region shown in (a) and (b).

3.5. Stability of folded GNIs

A stable folded structure is key to potential applications. To test the stability, a 2-ns MD simulation at RT is performed for the half-folded GNI without an external force. The initial and final structures are given in Fig. S8. It is found that the half-folded GNI with a random stacking mode (Fig. S8b in the ESM) transforms into a stable AB stacking configuration (Figs. S8c and S8d in the ESM). Comparing the configurations before and after the simulation, the folded GNI (Fig. S8c) slightly unfolds when we remove the external force. A folded GNI, with L_a smaller than 240 \AA , unfolds completely when the external force is removed. Above simulations suggest that unfolding barriers exist for half-folded GNIs.

The unfolding process is almost the reverse of the folding one. Therefore, the unfolding barrier (ΔE_p) can be extracted from the E_p evolution of the system at the last several picoseconds of the single-folding process. We amplify the potential energy of the GNI with L_a of 301 \AA in the last few picoseconds of the single-folding process (red rectangle in Fig. 6(a)) to demonstrate the feasibility of extracting ΔE_p from the folding process. The half-folded GNI is formed at 1080.2 ps. The corresponding configuration is shown in Fig. S8b. The potential energies show oscillation in the last few picoseconds. If the folded GNI overcomes the oscillation amplitude, it unfolds. Here, the unfolding barrier ΔE_p is described by the largest oscillation amplitude in the last few picoseconds.

The ΔE_p of the half-folded GNI is 2.64 eV , which is difficult to overcome at RT. It means if the half-folded GNI unfolds to the configuration at 1107.6 ps (Fig. S8a in the ESM), the unfolding process stops. The unfolded configuration is shown in

Fig. S8c after an MD simulation at 300 K for 2 ns. The configuration is very similar to the one at 1107.6 ps, supporting that the unfolding process is a reverse folding process. The folded structure (Fig. S8c) remains after a 4-ns MD simulation at 300 K (Fig. S8d), confirming a stable half-folded GNI

at RT. Besides, three GNIs with L_a s smaller than 301 Å are investigated, with their ΔE_p s summarized in Figs. 6(b)–6(d). It shows that the ΔE_p decreases as the L_a decreases, suggesting there is a critical size of the stable folded GNIs with decreasing ΔE_p .

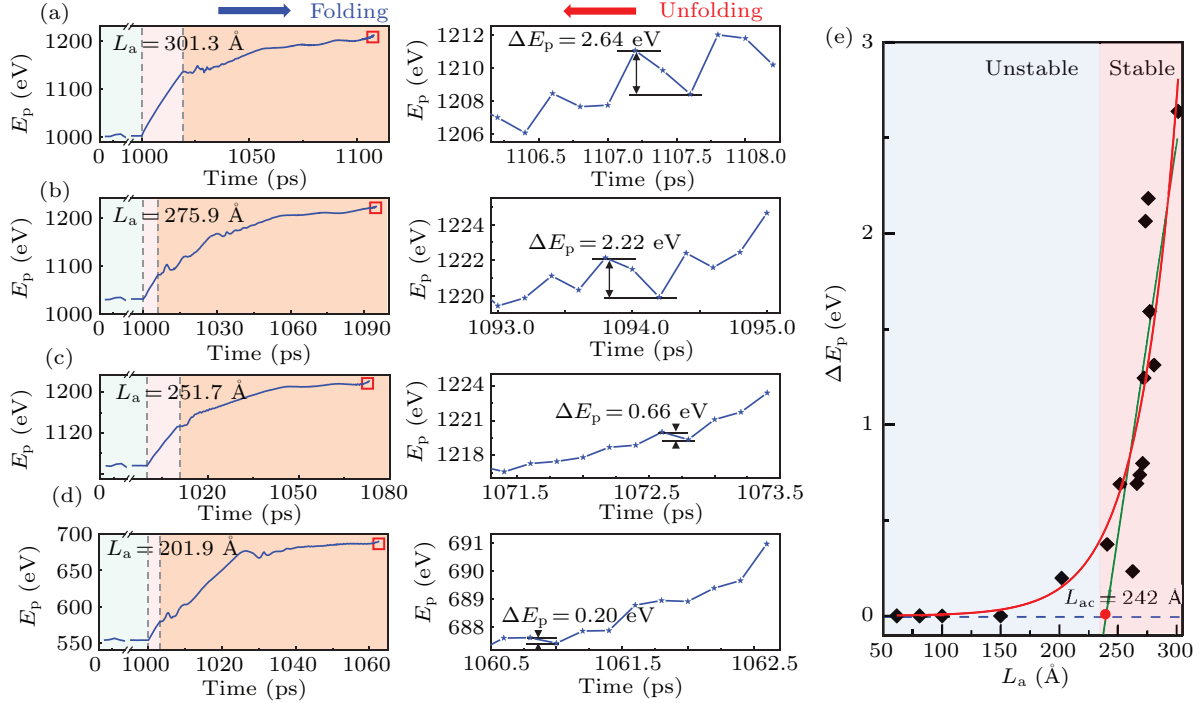


Fig. 6. Potential energy evolution and the stability of the folded GNIs with different sizes. (a)–(d) The potential energy evolution of GNIs with $L_a = 301.3$ Å, 275.9 Å, 251.7 Å, and 201.9 Å in the single-folding process (left panels) and the zoom-in figures of the red rectangles (right panels). (e) Unfolding barriers (ΔE_p s) of GNIs as a function of L_a ranging from 60 Å to 300 Å. The ΔE_p s of GNIs with L_a is fitted as a red line. The critical size (L_{ac}) of a stable folded GNI at RT is marked by a red dot.

To find out the critical size of the stable half-folded GNI at RT, we analyze the evolution of E_p of the single-folded GNIs with different L_a s ranging from 60 Å to 400 Å and extract the corresponding ΔE_p s. The ΔE_p exhibits an approximately exponential relationship with L_a as shown in Fig. 6(e). The ΔE_p is zero when the L_a of the folded GNI is less than 150 Å, indicating that the folded GNI prefers a spontaneous unfolding until it fully expands on the HOPG substrate. We perform MD simulations for these half-folded GNIs with L_a s smaller than 150 Å at RT and find that all of them unfold. When the L_a is larger than 250 Å, the ΔE_p is higher than 0.234 eV and increases quickly as the L_a increases, suggesting the unfolding process is unlikely to happen. MD simulations of these half-folded GNIs confirm their stability at RT. Given that the ΔE_p almost increases linearly with L_a , we fit a line across these points with L_a ranging from 250 Å to 300 Å, (green line in Fig. 6(e)). The intersection of the green line and the blue dashed line of $\Delta E_p = 0$ can be regarded as the critical size of a stable folded GNI structure. The critical size is $L_{ac} = 242$ Å. Then, we performed MD simulations of folded GNIs with L_a s of 241 Å, 247 Å and 249 Å at RT and found that the GNI with L_a of 241 Å unfolds while the rest two remains the folded con-

figuration. It further confirms that the critical size of the stable folded GNIs is around L_a of 242 Å.

Furthermore, we have performed computational analysis from a thermodynamic perspective and concluded that the critical size of the stable folded GNIs is between 240 Å and 250 Å (Table S1 in the ESM), which is consistent with the critical size (242 Å) obtained by fitting the unfolding barriers. In addition, the thermal stability of the folded GNI with $L_a = 300$ Å has been explored. It is found that the folded GNI is stable up to 1000 K (Fig. S9 in the ESM), indicating a good thermal stability.

4. Conclusion and perspectives

In summary, the process of GNI origami on a HOPG substrate is uncovered at the atomic scale by using SMD simulations. It is found that applying an external pulling force at a shaper armchair edge is optimal for realizing graphene origami. During the single-folding process, the potential energy of GNI firstly increases due to the formation of the curved region and then decreases as the vdW stacking region forms. Comparing the RDF of the curved region with the unfolded GNI and the bond-length evolution in the origami process, we

find that the sp^2 hybridization of the carbon atoms retains during the folding process. It is worth noting that the folded GNI with L_a larger than 242 Å is stable at RT and changes to an AB stacking mode when the external force is removed. These findings are helpful to better understanding the mechanism and structure evolution in the GNI origami process. It paves the way for pursuing other 2D materials origami and provides a guide to preparing origami-based nanodevices in experiments.

Acknowledgements

Project supported by the National Natural Science Foundation of China (Grant Nos. 61888102 and 52102193), the Strategic Priority Research Program of the Chinese Academy of Sciences (Grant No. XDB30000000), and the Fundamental Research Funds for the Central Universities. Computational resources were provided by the National Supercomputing Center in Tianjin.

References

- [1] Ning X, Wang X, Zhang Y, Yu X, Choi D, Zheng N, Kim D S, Huang Y, Zhang Y and Rogers J A 2018 *Adv. Mater. Interfaces* **5** 1800284
- [2] Chen S, Chen J, Zhang X, Li Z Y and Li J 2020 *Light Sci. Appl.* **9** 99
- [3] Zhang Z, Tian Z, Mei Y and Di Z 2021 *Mater. Sci. Eng. R Rep.* **145** 100621
- [4] Jamalimehr A, Mirzajanzadeh M, Akbarzadeh A and Pasini D 2022 *Nat. Commun.* **13** 1816
- [5] Queisser F and Schützhold R 2013 *Phys. Rev. Lett.* **111** 046601
- [6] Wang Z, Jing L, Yao K, Yang Y, Zheng B, Soukoulis C M, Chen H and Liu Y 2017 *Adv. Mater.* **29** 1700412
- [7] Zhao G, Mu H, Liu F and Wang Z 2020 *Nano Lett.* **20** 5860
- [8] Li S Y, Su Y, Ren Y N and He L 2020 *Phys. Rev. Lett.* **124** 106802
- [9] Wei N, Chen Y, Cai K, Zhang Y, Pei Q, Zheng J C, Mai Y W and Zhao J 2022 *Green Energy Environ.* **7** 86
- [10] Ho D T, Park H S, Kim S Y and Schwingenschlöggl U 2020 *ACS Nano* **14** 8969
- [11] Yang H and Ma L 2020 *Mater. Des.* **188** 108430
- [12] Becker C, Bao B, Karanashenko D D, Bandari V K, Rivkin B, Li Z, Faghieh M, Karanashenko D and Schmidt O G 2022 *Nat. Commun.* **13** 2121
- [13] Lee W, Liu Y, Lee Y, Sharma B K, Shinde S M, Kim S D, Nan K, Yan Z, Han M and Huang Y 2018 *Nat. Commun.* **9** 1417
- [14] Han E, Yu J, Annevelink E, Son J, Kang D A, Watanabe K, Taniguchi T, Ertekin E, Huang P Y and van der Zande A M 2020 *Nat. Mater.* **19** 305
- [15] Chang J S, Kim S, Sung H J, Yeon J, Chang K J, Li X and Kim S 2018 *Small* **14** 1803386
- [16] Shi L J, Yang L Z, Deng J Q, Tong L H, Wu Q, Zhang L, Zhang L, Yin L J and Qin Z 2020 *Carbon* **165** 169
- [17] Chen H, Zhang X L, Zhang Y Y, Wang D, Bao D L, Que Y, Xiao W, Du S, Ouyang M and Pantelides S T 2019 *Science* **365** 1036
- [18] Xu W, Qin Z, Chen C T, Kwag H R, Ma Q, Sarkar A, Buehler M J and Gracias D H 2017 *Sci. Adv.* **3** e1701084
- [19] He Z Z, Zhu Y B and Wu H A 2018 *Front. Phys.* **13** 138111
- [20] Annett J and Cross G L 2016 *Nature* **535** 271
- [21] Zang X, Shen C, Chu Y, Li B, Wei M, Zhong J, Sanghadasa M and Lin L 2018 *Adv. Mater.* **30** 1800062
- [22] Dai Z, Liu L and Zhang Z 2019 *Adv. Mater.* **31** 1805417
- [23] Wang Y and Crespi V H 2017 *Nano Lett.* **17** 6708
- [24] Reynolds M F, McGill K L, Wang M A, Gao H, Mujid F, Kang K, Park J, Miskin M Z, Cohen I and McEuen P L 2019 *Nano Lett.* **19** 6221
- [25] Fan X, Kim S W, Tang J, Huang X, Lin Z, Zhu L, Li L, Cho J H and Zeng C 2021 *Nano Lett.* **21** 2033
- [26] Zhu S and Li T 2014 *ACS Nano* **8** 2864
- [27] Zhang L, Zeng X and Wang X 2013 *Sci. Rep.* **3** 3162
- [28] Ho D T, Ho V H, Babar V, Kim S Y and Schwingenschlöggl U 2020 *Nanoscale* **12** 10172
- [29] Wei N, Chen Y, Zhang Y, Zheng J C, Zhao J and Mai Y W 2020 *Carbon* **165** 259
- [30] Yang Y, Zhang Z, Hu Z, Penev E S and Yakobson B I 2021 *MRS Bull.* **46** 481
- [31] Rico F, Gonzalez L, Casuso I, Puig-Vidal M and Scheuring S 2013 *Science* **342** 741
- [32] Qi J, Gao Y, Jia H, Richter M, Huang L, Cao Y, Yang H, Zheng Q, Berger R and Liu J 2020 *J. Am. Chem. Soc.* **142** 10673
- [33] Wang J, Wolf R M, Caldwell J W, Kollman P A and Case D A 2004 *J. Comput. Chem.* **25** 1157
- [34] Abraham M J, Murtola T, Schulz R, Pall S, Smith J C, Hess B and Lindahl E 2015 *SoftwareX* **1-2** 19
- [35] Kim K, Lee Z, Malone B D, Chan K T, Alemán B, Regan W, Gannett W, Crommie M, Cohen M L and Zettl A 2011 *Phys. Rev. B* **83** 245433
- [36] Zhang J, Xiao J, Meng X, Monroe C, Huang Y and Zuo J M 2010 *Phys. Rev. Lett.* **104** 166805
- [37] Levine B G, Stone J E and Kohlmeyer A 2011 *J. Comput. Phys.* **230** 3556